JOURNAL OF CHEMICAL & ENGINEERING DATA

ARTICLE

pubs.acs.org/jced

Transport Properties of *N*-Butyl-*N*-methylpyrrolidinium Bis(trifluoromethylsulfonyl)amide

Kenneth R. Harris* and Lawrence A. Woolf

School of Physical, Environmental and Mathematical Sciences, University College, University of New South Wales, Australian Defence Force Academy, P.O. Box 7916, Canberra BC, ACT 2610 Australia

Mitsuhiro Kanakubo

National Institute of Advanced Industrial Science and Technology (AIST), 4-2-1 Nigatake, Miyagino-ku, Sendai 983-8551, Japan

Thomas Rüther

Commonwealth Scientific and Industrial Research Organisation, Energy Technology, P.O. Box 312, Clayton South, Victoria 3169, Australia

ABSTRACT: The viscosities (η) and ion self-diffusion coefficients (D_i) of the ionic liquid *N*-butyl-*N*-methylpyrrolidinium bis(trifluoromethylsulfonyl)amide ([Pyr_{14}][Tf_2N] or [C_4mpyr][Tf_2N]) are reported between (0 and 90) °C and at pressures to 103 MPa and between (25 and 80) °C to 250 MPa, respectively. A falling-body high-pressure viscometer was employed, supplemented by a Stabinger rotating-cylinder viscometer for atmospheric pressure. Self-diffusion coefficients were measured by the steady-gradient spin−echo NMR technique. The overall uncertainties are ± 2 % and ± 3 %, respectively. Conductivities (κ) and densities obtained between (0 and 90) °C at 0.1 MPa are reported. Ion self-diffusion coefficients and densities at 0.1 MPa are included for *N*-methyl-*N*-propyl-3-azabicyclo[3.2.2]nonaneium bis(trifluoromethylsulfonyl)amide ([3-ABN_{13}][Tf_2N]). The transport properties are examined using the fractional Stokes−Einstein and Nernst−Einstein relations, velocity correlation coefficients, and density scaling. For [Pyr_{14}][Tf_2N], the fractional Stokes−Einstein exponents are (0.93 ± 0.05). There is very good consistency between the diffusion and molar conductivity (Λ) data, with a slope of (0.99 ± 0.05) for a plot of $\ln(T\Lambda)$ against $\ln(D_+ + D_-)$. The Nernst−Einstein deviation parameter, Δ, is (0.313 ± 0.013): it is consistent with the relation $f_{+-} > (f_{++} + f_{--})/2$ for the ion−ion velocity cross-correlation coefficients, f_{ij}. Density scaling to the temperature-volume function (TV^{γ}) has been applied to both unreduced and reduced viscosities and self-diffusion coefficients for [Pyr_{14}][Tf_2N]. Consistent scaling parameters γ are obtained for each of η, D_+, and D_- with both the Casalini-Roland model and a simple polynomial fit in (TV^{γ}), and for the reduced quantities, $\tilde{\eta}$, $\tilde{D}_+$, and $\tilde{D}_-$. At a fixed temperature, the self-diffusion coefficients for the series [BMIM][Tf_2N], [Pyr_{14}][Tf_2N], and [3-ABN_{13}][Tf_2N] decrease with increasing salt molar volume, but the ratio of D(cation) to D(anion) changes from values greater than unity to less than unity, in common with what is generally observed for ionic liquid families.

INTRODUCTION

This work continues a series on the transport properties of ionic liquids at high pressure.[1−7] One such liquid, of interest as an electrolytic solvent for certain electrochemical processes under study at CSIRO Energy Technology, is *N*-butyl-*N*-methylpyrrolidinium [or 1-butyl-1-methylpyrrolidinium] bis-(trifluoromethylsulfonyl)amide ([Pyr_{14}][Tf_2N] or [C_4mpyr]-[Tf_2N]).[8] This ionic liquid has a very broad electrochemical window, of approximately 5.5 V, about 2 V broader than those of conventional imidazolium-based ionic liquids, making it suitable for applications at extreme electrochemical potentials.[9] The electrodeposition of aluminum metal from $AlCl_3$ solutions in [Pyr_{14}][Tf_2N] has been studied, along with ion speciation, as part of work at CSIRO on alternatives to the standard commercial methods of aluminum production and electroplating.[10,11] [Pyr_{14}][Tf_2N] has also been investigated as an electrolytic solvent in rechargeable lithium batteries.[12,13]

As in our earlier studies we report high-pressure viscosities and ion self-diffusion coefficients, using literature *pVT* data for the analysis of the data.[14,15] Densities and conductivities are also reported, but only for atmospheric pressure. This work is aimed at obtaining more information about the relationships between the transport properties in this material.

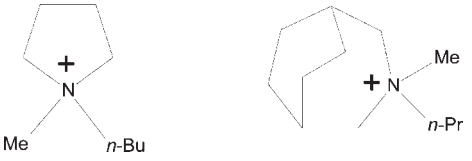

Figure 1. Structures of the *N*-butyl-*N*-methylpyrrolidinium and the *N*-methyl-*N*-propyl-3-azabicyclo[3.2.2]nonaneium cations.

Though [Pyr_{14}][Tf_2N] is the material of primary interest in this work, densities and ion self-diffusion coefficients at

Special Issue: Kenneth N. Marsh Festschrift

Received: June 29, 2011
Accepted: August 6, 2011
Published: September 21, 2011

dx.doi.org/10.1021/je2006049 | *J. Chem. Eng. Data* 2011, 56, 4672–4685

Table 1. Ionic Liquid Samples

	M/g·mol^{-1}	CAS no.	sample	purity (mole fraction)	property measured	$10^6 \cdot w$ (H_2O)	$10^6 \cdot w$ (M^+,X^-)
$[Pyr_{14}][Tf_2N]$	422.4055	223 437-11-4	#1, Merck 491046 lot eq 407146 618	> 0.99[a,b]	D (atm p)	< 100,[a] 45[c]	< 100[a]
			#2, Merck 492046 lot S4847346 735	> 0.99[a,b]	ρ, D (atm p)	200,[a] 150[c]	< 10 (X^-)[a]
			#3, Merck 492046 lot LS8040746 814	0.996[a,b]	ρ,D,η	6,[a] 40[c]	< 10 (X^-)[a]
			# 4, Kanto	> 0.999[d]	ρ,η,Λ	3.6[a]	0.1 (K^+)[a] < 0.1 (other metals) < 1 (F^-, Cl^-, Br^-)
$[3\text{-}ABN_{13}][Tf_2N]$	462.4694	1002717-87-4	0054.2ABN	> 0.999[d]	ρ,D (atm p)	26[c]	0.2 (Li^+), 9 (I^-)[e]

[a] Manufacturer's analysis. [b] NMR analysis. [c] Our analysis. [d] Best estimate, based on analyses for water and specific ionic impurities, as listed. [e] ICP and IC analyses respectively.

atmospheric pressure are included for *N*-methyl-*N*-propyl-3-azabicyclo[3.2.2]nonaneium bis(trifluoromethylsulfonyl)amide ($[3\text{-}ABN_{13}][Tf_2N]$). This is also a candidate electrolyte for rechargeable lithium batteries, the cation (Figure 1) being originally introduced for the study of structure−property relationships.[16] It also has a very broad electrochemical window, of approximately 6.1 V.[16] Unfortunately, there was insufficient material available to determine conductivities or viscosities, but the diffusion data do allow a limited examination of the affects of cation structure on diffusion in $[Tf_2N]^-$ salts.

As in our earlier studies,[3,7] the results are discussed in terms of the fractional Stokes−Einstein and Nernst−Einstein relations and velocity correlation coefficients. In addition the analysis is extended to include "thermodynamic" or "density" scaling.[17−19]

EXPERIMENTAL SECTION

$[Pyr_{14}][Tf_2N]$ samples were obtained from Merck Australia and the Kanto Chemical Co., Japan. The $[3\text{-}ABN_{13}][Tf_2N]$ sample was prepared in the CSIRO Energy Technology laboratory by methods similar to those given by Rüther et al.[16,20] The purities, CAS numbers and molar masses are given in Table 1. Water contents were determined by Karl Fischer titration using a Metrohm 831 KF Coulometer.

The falling body viscometer (Canberra laboratory) and its calibration and operation with ionic liquids have been described previously.[1,2,5,6] The viscometer cell (volume, 13 mL) was loaded and sealed within a drybox. The working equation is

$$\eta(p,T) = \frac{t(1-\rho/\rho_s)}{A[(1+2\alpha(T-T_{ref})][1-2\beta(p-p_{ref})/3]} \quad (1)$$

where η is the shear viscosity, t is the fall time, ρ is the density of the fluid, ρ_s is that of the sinker, α is the coefficient of thermal expansion, and β is the bulk compressibility of the sinker and tube material, in this case 316 stainless steel. A is the calibration constant, determined with high viscosity Cannon standards. It is independent of temperature and viscosity. The sinker densities were corrected for changes in T and p from the reference state point, T_{ref} = 298.15 K and p_{ref} = 0.1 MPa using the relation:

$$\rho_s = \frac{\rho_s(T_{ref},p_{ref})}{[1+3\alpha(T-T_{ref})][1-\beta(p-p_{ref})]} \quad (2)$$

The viscometer tube and sinker diameters are (6.52 and 6.0) mm, respectively. The Reynolds number for annular flow in a viscometer of this type is given by

$$Re = 2r_1{}^2\rho v/((r_2-r_1)\eta) \quad (3)$$

where v is the terminal velocity of the sinker and r_1 and r_2 are the radii of the sinker and tube, respectively. The expanded uncertainty is estimated at ± 2 %.

The steady gradient spin−echo NMR method was used in the Canberra laboratory to determine the ionic self-diffusion coefficients using the proton resonance for the cations and the fluorine resonance for the anions. Calibration of the quadrupole magnetic field gradient coils was carried out with water and benzene using established methods.[3,21−23] For the IL measurements, only the magnetic field gradient was varied, through both positive and negative ranges (± 80 μT·m^{-1}·rad^{-1}), at constant 90° to 180° pulse spacing [(35 to 65) ms], due to the short T_2 relaxation times which are of similar order to the pulse intervals and can depend strongly on temperature and pressure for ionic liquids. Dried samples were loaded into flamed standard 5 mm NMR tubes in a drybox for the atmospheric pressure measurements. These were inserted into a cylindrical, ceramic coil former on which are cemented both gradient and rf transmitter-receiver coils. The coil former sits in a small bath containing a fluid with nonresonant nuclei (3M FC-75 Fluorinert for proton resonance and methylcyclohexane for fluorine resonance): this bath is heated or cooled from an external Julabo circulating thermostat. Teflon bellows cells were used for the high pressure measurements and were also loaded in a drybox. These were similarly inserted into a ceramic combined rf and gradient coil former contained within a Be−Cu pressure vessel. This was surrounded by a dewar containing oil heated or cooled by the external thermostat. Temperature control was ± 20 mK. FC-75 was used as the hydraulic fluid in the high pressure system for proton resonance and plexol [bis(2-ethylhexyl) decanedioate] for the fluorine resonance. The diffusion cells (volume, 7 mL) were loaded, stored and sealed within the drybox. The expanded uncertainty is ± 3 %.

Conductivities (κ) were determined for the Kanto Chemical Co $[Pyr_{14}][Tf_2N]$ sample with a Bio-Logic SP-150 impedance analyzer in the Sendai laboratory.[24] A syringe-type cell with a pair of bright platinum electrodes was employed as previously described.[3,4] The cell constant was 0.354 cm^{-1} at 25 °C and

Table 2. Densities ρ of Ionic Liquids from θ = (0 to 90) °C[a]

θ/°C	$[Pyr_{14}][Tf_2N]$ sample 2	$[Pyr_{14}][Tf_2N]$ sample 3	$[Pyr_{14}][Tf_2N]$ sample 4[b]	$[3\text{-}ABN_{13}]$ $[Tf_2N]$
0.00	1.41689	1.41694	1.4167	1.42591
5.00			1.4121	
10.00	1.40776	1.40782	1.4076	1.41720
15.00		1.40339	1.4032	
20.00	1.39892	1.39896	1.3987	1.40855
20.00			1.3988	
25.00	1.39451		1.3944	1.40434
25.00				1.40423
25.00				1.40430
30.00	1.39010	1.39017	1.3900	1.39993
40.00	1.38131	1.38138	1.3812	1.39131
50.00	1.37258	1.37267	1.3725	1.38285
60.00	1.36389	1.36397	1.3639	1.37484
60.00				1.37460
60.00				1.37453
70.00	1.35526	1.35536	1.3553	1.36629
70.00				1.36665
70.00				1.36657
70.00				1.36665
80.00	1.34669	1.34678	1.3468	1.35843
80.00				1.35835
90.00	1.33816	1.33825	1.3384	1.35025
90.00				1.35026

[a] Density units, $g \cdot cm^{-3}$; standard uncertainties u are $u(T) = 0.01$ K and $u(\rho) = 0.0001$ $g \cdot cm^{-3}$ for the DMA5000 measurements and $u(T) = 0.02$ K and $u(\rho)$ 0.0005 $g \cdot cm^{-3}$ for the Stabinger unit measurements. [b] Stabinger unit.

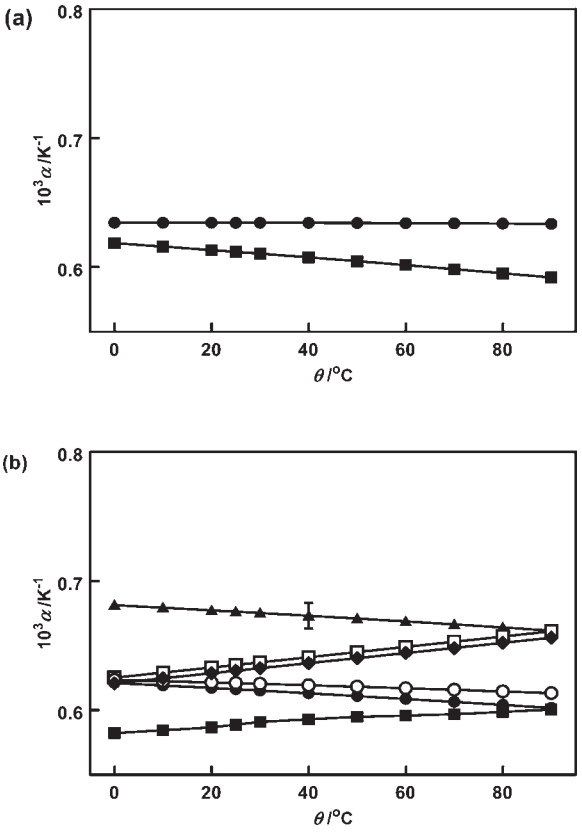

Figure 2. (a) Thermal expansivities as a function of Celsius temperature, θ. symbols: ●, $[Pyr_{14}][Tf_2N]$; ■, $[3\text{-}ABN_{13}][Tf_2N]$; (b) symbols: ●, $[BMIM][PF_6]$; ◆, $[HMIM][PF_6]$; ○, $[OMIM][PF_6]$; ■, $[BMIM][BF_4]$; □, $[OMIM][BF_4]$;▲, $[BMIM][Tf_2N]$.

was corrected at different temperatures by taking into account the known thermal expansion coefficients of glass and platinum. The solution resistance was obtained from the Nyquist plot by fitting the measured impedances to the best-fit form of an arbitrary electric circuit. Both potentiometric and galvanometric procedures gave the same result within experimental error. The expanded uncertainty is ± 2 %.

Differential scanning calorimetry (DSC) was performed with a Bruker DSC3200 unit (Sendai), using a tared aliquot (~ 11 mg) of $[Pyr_{14}][Tf_2N]$, weighed within a drybox and sealed in an aluminum pan. The DSC trace was recorded using a similar amount of Al_2O_3 reference material at a scan rate of 5 K min^{-1}. Dry nitrogen gas was slowly passed through the DSC chamber during the measurements. The sample was cooled from 25 °C down to −120 °C and then heated to 100 °C. This temperature cycle was repeated twice and the glass transition was determined from the second cycle. Densities at atmospheric pressure were determined with an Anton-Paar DMA5000 vibrating tube densimeter in the Canberra laboratory as described previously.[1,2] The in-built viscosity correction for this instrument has been confirmed in earlier work.[1,2] As before, the glass vibrating tube was carefully rinsed with filtered ethanol, acetone and dry air before being loaded with ionic liquid (volume required, 5−10 mL, including flushing). The expanded uncertainty is ± 0.0001 $g \cdot cm^{-3}$.[25]

Densities and viscosities for the Kanto Chemical Co $[Pyr_{14}][Tf_2N]$ sample were also measured in the Sendai laboratory, as a check, using an Anton Paar Stabinger SVM 3000 rotating-cylinder viscometer, which incorporates a vibrating tube densimeter, also with an automated viscosity correction. The expanded uncertainties are estimated at ± 2 % for the viscosity and ± 0.0005 $g \cdot cm^{-3}$ for the density.

Calculation of the viscosity from fall times requires knowledge of the density as a function of temperature and pressure. The pVT data for $[Pyr_{14}][Tf_2N]$ of Gardas et al.[14] [(20 to 120) °C, p_{max} = 35 MPa] and of Jacquemin et al.[15] [(20 to 142) °C, p_{max} = 40 MPa] were fitted to the Tait equation

$$V = V_0\{1 - C\ln[(B(T) + p)/(B(T) + p_0)]\} \quad (4)$$

as a function of temperature and pressure. V_0 is the molar volume at the saturation pressure, p_0, for a given temperature, T. C = (0.0841 ± 0.021) and $B(T)$/MPa = (264.3 ± 69) − (0.3500 ± 0.087)T/K.

This equation reproduces the densities within the measurement ranges of T and p with a standard deviation of ± 0.07 %: it has been found to be superior to the Hayward equation, used in previous studies,[1,3−6] when long extrapolations are required, as in the scaling calculations discussed below.[26]

High pressure densities needed for the viscosity measurements were then calculated using our atmospheric pressure densities and eq 4. As the sinker is 5 to 7 times denser than the ionic liquids used in this study, it is sufficient if the density is known to better than 5 % for an overall uncertainty in the viscosity of 1 % as it enters the viscosity calculation (eq 1) in terms of the buoyancy factor $(1 - \rho/\rho_s)$. The uncertainty in

Table 3. (a) Viscosity η of $[Pyr_{14}][Tf_2N]$ from θ = (0 to 80) °C and p = (0.1 to 103) MPa (Falling-Body Viscometer, 6.0 mm Sinker)[a] and (b) Viscosity η of $[Pyr_{14}][Tf_2N]$ from θ = (0 to 90) °C (Stabinger Viscometer)[b]

(a)

θ/°C	p/MPa	V/(cm^{3}mol^{-1})	ρ/(g·cm^{-3})	t/s	η/(mPa·s)	Re[c]
0.00	0.10	298.13	1.41684	1003	319.28	0.031
0.00	0.10	298.13	1.41684	1002	318.72	0.031
0.00	0.10	298.13	1.41684	1007	320.44	0.030
0.00	0.82	298.03	1.41735	1000	318.29	0.031
0.00	10.85	296.59	1.42423	1190	378.12	0.022
0.00	20.76	295.24	1.43072	1392	441.79	0.016
0.00	32.19	293.77	1.43787	1710	542.04	0.011
0.00	40.24	292.79	1.44270	1962	621.51	0.0082
0.00	45.00	292.22	1.44548	2139	677.25	0.0069
0.00	50.31	291.61	1.44853	2305	729.34	0.0060
0.00	59.20	290.61	1.45350	2649	837.70	0.0045
0.00	60.55	290.46	1.45424	2707	855.99	0.0043
0.00	69.28	289.53	1.45895	3114	983.67	0.0033
0.00	70.31	289.42	1.45949	3193	1008.74	0.0031
0.00	80.52	288.37	1.46479	3754	1184.76	0.0023
5.00	0.10	299.08	1.41235	706.4	224.84	0.062
5.00	0.10	299.08	1.41235	706.4	224.85	0.062
10.00	0.10	300.03	1.40788	522.9	166.57	0.11
10.00	0.10	300.03	1.40788	524.9	167.15	0.11
10.00	0.10	300.03	1.40788	524.9	167.15	0.11
10.00	0.10	300.03	1.40788	524.6	167.09	0.11
10.00	0.10	300.03	1.40788	524.6	167.09	0.11
10.00	0.10	300.03	1.40788	522.9	166.56	0.11
10.00	10.14	298.54	1.41489	604.9	192.43	0.084
10.00	19.97	297.17	1.42143	701.6	222.97	0.063
10.00	29.99	295.84	1.42781	816.5	259.18	0.047
10.00	40.62	294.50	1.43430	956.5	303.30	0.034
10.00	50.52	293.32	1.44009	1106	350.45	0.026
10.00	59.77	292.26	1.44531	1260	398.94	0.020
10.00	70.19	291.12	1.45097	1465	463.39	0.015
10.00	78.71	290.22	1.45545	1637	517.26	0.012
10.00	89.72	289.11	1.46106	1966	620.70	0.0083
10.00	89.96	289.09	1.46118	1914	604.22	0.0087
10.00	100.39	288.08	1.46630	2248	708.87	0.0064
10.00	100.39	288.08	1.46630	2227	702.53	0.0065
20.00	0.10	301.94	1.39897	313.1	99.81	0.31
20.00	0.10	301.94	1.39897	313.4	99.92	0.31
25.00	0.10	302.90	1.39454	239.9	76.54	0.53
25.00	0.10	302.90	1.39454	246.2	78.55	0.50
25.00	0.10	302.90	1.39454	246.0	78.48	0.50
25.00	0.10	302.90	1.39454	239.9	76.53	0.53
25.00	0.10	302.90	1.39454	240.2	76.63	0.52
25.00	0.86	302.78	1.39510	242.1	77.22	0.52
25.00	10.37	301.32	1.40187	276.1	87.96	0.40
25.00	20.76	299.81	1.40892	317.1	100.93	0.30
25.00	30.70	298.45	1.41535	361.6	114.96	0.24
25.00	40.66	297.15	1.42152	411.2	130.58	0.18
25.00	50.63	295.92	1.42745	467.3	148.26	0.14
25.00	60.60	294.74	1.43315	529.9	167.95	0.11
25.00	70.39	293.63	1.43855	598.3	189.46	0.088
25.00	80.18	292.57	1.44376	675.6	213.75	0.069

Table 3. Continued

(a)

θ/°C	p/MPa	V/(cm^{3}mol^{-1})	ρ/(g·cm^{-3})	t/s	η/(mPa·s)	Re[c]
25.00	90.60	291.49	1.44911	766.1	242.18	0.054
25.00	100.23	290.53	1.45390	859.9	271.62	0.043
30.00	0.10	303.86	1.39013	196.8	62.82	0.78
30.00	0.10	303.86	1.39013	196.2	62.63	0.78
40.00	0.10	305.79	1.38134	129.1	41.27	1.8
40.00	0.10	305.79	1.38134	129.1	41.24	1.8
50.00	0.10	307.74	1.37260	90.84	29.06	3.6
50.00	0.10	307.74	1.37260	90.76	29.04	3.6
50.00	0.10	307.74	1.37260	89.50	28.63	3.7
50.00	0.10	307.74	1.37260	90.84	29.05	3.6
50.00	0.10	307.74	1.37260	90.76	29.03	3.6
50.00	0.10	307.74	1.37260	89.50	28.63	3.7
50.00	10.52	306.02	1.38033	101.1	32.31	2.9
50.00	20.60	304.46	1.38741	113.5	36.21	2.3
50.00	29.97	303.08	1.39370	126.0	40.16	1.9
50.00	39.91	301.70	1.40008	140.5	44.72	1.5
50.00	50.59	300.30	1.40663	157.4	50.06	1.2
50.00	60.55	299.05	1.41249	175.4	55.73	1.0
50.00	70.49	297.86	1.41811	194.6	61.77	0.81
50.00	80.45	296.73	1.42355	215.2	68.24	0.67
50.00	90.47	295.63	1.42882	237.8	75.36	0.55
50.00	100.40	294.59	1.43385	262.1	82.99	0.46
60.00	0.10	309.70	1.36392	66.55	21.31	6.7
60.00	0.10	309.70	1.36392	66.51	21.30	6.7
70.00	0.10	311.67	1.35530	50.37	16.14	12
70.00	0.10	311.67	1.35530	50.33	16.13	12
75.00	0.10	312.66	1.35101	43.87	14.07	15
75.00	0.10	312.66	1.35101	43.83	14.06	15
75.00	10.85	310.75	1.35932	48.97	15.68	12
75.00	11.99	310.55	1.36017	49.41	15.82	12
75.00	21.76	308.94	1.36726	54.84	17.54	9.8
75.00	29.21	307.78	1.37244	58.83	18.80	8.6
75.00	38.02	306.46	1.37833	63.83	20.38	7.3
75.00	49.60	304.83	1.38571	71.83	22.90	5.8
75.00	64.63	302.85	1.39477	83.09	26.45	4.4
75.00	73.06	301.80	1.39962	89.39	28.44	3.8
75.00	85.04	300.38	1.40624	99.22	31.53	3.1
75.00	102.92	298.39	1.41560	116.0	36.80	2.3
80.00	0.10	313.65	1.34674	39.68	12.73	18
80.00	0.10	313.65	1.34674	39.49	12.67	19

(b)

θ/°C	η/(mPa·s)	θ/°C	η/(mPa·s)
0.00	322.4	30.00	62.26
5.00	230.9	40.00	41.72
10.00	170.1	50.00	29.42
15.00	128.4	60.00	21.64
20.00	98.95	70.00	16.46
20.00	99.00	80.00	12.91
25.00	77.83	90.00	10.35

[a] Standard uncertainties u are $u(T)$ = 0.01 K, $u(p)$ = 0.2 MPa above 1 MPa and $u(\eta)$ = 2 %. [b] Standard uncertainties u are $u(T)$ = 0.02 K and $u(\eta)$ = 2 %. [c] Reynolds number.

dx.doi.org/10.1021/je2006049 |J. Chem. Eng. Data 2011, 56, 4672–4685

Table 4. (a) $[Pyr_{14}][Tf_2N]$: Coefficients of Best Fit for eqs 7 and 8 and Their Analogues and (b) $[3\text{-}ABN_{13}][Tf_2N]$: Coefficients of Best Fit for the Analogue of eq 7

	η/mPa·s	(a) $10^{12}D_+/m^2\cdot s^{-1}$	$10^{12}D_-/m^2\cdot s^{-1}$	$\Lambda/\mu S\cdot m^2\cdot mol^{-1}$
ln (A/mPa·s)	−0.23347 ± 0.0086	7.4630 ± 0.015	7.4253 ± 0.023	8.6590 ± 0.022
$B\cdot10^{-6}$/K	121.817 ± 0.23	−122.802 ± 0.47	−126.461 ± 0.78	−112.659 ± 0.61
standard uncertainty of fit/%	1.4	1.7	2.0	1.8
ln (A'/mPa·s)	−1.9760 ± 0.059	9.4303 ± 0.024	10.199 ± 0.39	9.96898 ± 0.0082
B'/K	867.6 ± 17	−934.0 ± 79	−1227.3 ± 147	−716.53 ± 2.2
T_0/K	161.03 ± 1.4	156.61 ± 6.9	135.2 ± 11	168.9024 ± 0.021
δ^a	5.39	−5.96	−9.08	−4.242
standard uncertainty of fit/%	1.1	1.6	1.6	0.08

	(b) $10^{12}D_+/m^2\cdot s^{-1}$	$10^{12}D_-/m^2\cdot s^{-1}$
ln (A/mPa·s)	7.979 ± 0.11	7.7346 ± 0.091
$B\cdot10^{-6}$/K	−197.96 ± 4.5	−185.33 ± 3.7
standard uncertainty of fit/ %	1.5	1.2

[a] Angell strength factor (B'/T_0).

densities estimated from eq 4 is probably of the order of ± 0.5 % to 1 %, increasing with increasing pressure.

RESULTS AND DISCUSSION

a. Density. The density results at atmospheric pressure are presented in Table 2 and can be represented by the polynomials

$$\rho([Pyr_{14}][Tf_2N])/g\cdot cm^{-3} = (1.416\,834 \pm 0.000\,031) - (8.989\,3 \pm 0.016)\cdot10^{-4}(\theta/^\circ C) + (2.832 \pm 0.18)\cdot10^{-7}(\theta/^\circ C)^2 \quad (5)$$

$$\rho([3\text{-}ABN_{13}][Tf_2N])/g\cdot cm^{-3} = (1.425\,977 \pm 0.000\,088) - (8.821\,8 \pm 0.042)\cdot10^{-4}(\theta/^\circ C) + (4.600 \pm 0.43)\cdot10^{-7}(\theta/^\circ C)^2 \quad (6)$$

where θ is the Celsius temperature, with standard uncertainties of fit of (± 0.000 06 and ± 0.000 12) g·cm^{-3}, respectively. The densities from $[Pyr_{14}][Tf_2N]$ samples 2 and 3, measured with the DMA5000 densimeter, differed negligibly, despite the different water content, and eq 5 represents both sets. The densities for sample 4, measured with the Stabinger unit, agree within the combined experimental uncertainties (Table 2). Our results for $[Pyr_{14}][Tf_2N]$ are in fair agreement with those of Jacquemin et al.,[15] who have comprehensively summarized earlier work (mean bias = −0.000 25 g·cm^{-3}, comparable with the combined uncertainty of ± 0.000 15 g·cm^{-3}, our data being the higher) and in excellent agreement with those of Pereiro et al.[27] (mean bias = 0.000 03 g·cm^{-3}) and of Kolbeck et al.[28] (mean bias = −0.000 24 g·cm^{-3}), who also used DMA 5000 vibrating tube densimeters. There is also fair agreement with the Stabinger results of Shamsipur et al.[29] (stand devn = 0.002 g·cm^{-3}). There appear to be no published density data for $[3\text{-}ABN_{13}][Tf_2N]$.

The thermal expansivities of ionic liquids are of some interest[30] as some have been found with negative temperature coefficients, i.e., $(\partial\alpha_p/\partial T)_p < 0$, which implies $(\partial C_p/\partial p)_T > 0$, a relation not normally obeyed by molecular liquids. Of the liquids studied here, $[3\text{-}ABN_{13}][Tf_2N]$ has such a negative temperature coefficient, whereas $[Pyr_{14}][Tf_2N]$ shows typical behavior, with $(\partial\alpha_p/\partial T)_p \sim 0$ (Figure 2a). From our previous work,[1,2,5,6] [BMIM][BF_4], [OMIM][BF_4], and [HMIM][PF_6] have small, positive temperature coefficients for the thermal expansivities, that for [OMIM][PF_6] is close to 0 and those for [BMIM]-[Tf_2N] and [BMIM][PF_6] are small and negative (Figure 2b).

b. Viscosity. The viscosities are presented in Table 3. Good agreement was obtained between the two Merck samples (2 and 3) measured with the falling body viscometer in Canberra and the Kanto sample (4) measured with the Stabinger instrument in Sendai. Together with the excellent agreement for the densities, this argues for the equivalence of the two manufacturers' samples. No measurements could be made for $[3\text{-}ABN_{13}]$-$[Tf_2N]$ due to insufficient material being available.

As in our previous studies, data were fitted to the Litovitz equation

$$\eta = A\exp(B/RT^3) \quad (7)$$

and the Vogel−Fulcher−Tammann (VFT) equation

$$\eta = A'\exp(B'/(T - T_0)) \quad (8)$$

The coefficients are given in Table 4. The VFT coefficients are consistent with the Angell relationship for D ($\equiv B'/T_0$), T_0 and the glass temperature T_g, based on the scaling of the (coexistence line) viscosities of a wide range of liquids in the range $0 < (T_g/T_0) < 1$, with the assumption of a common single viscosity value (η_g) at T_g.[31] Thus

$$T_g/T_0 = 1 + D/(2.303\log(\eta_g/\eta_0)) \quad (9)$$

where Angell found $\log(\eta_g/\eta_0)$ empirically to be about 17. Our data predict a T_g of 183.2 K, in good agreement with the value obtained from DSC measurements, 182 K: other direct measurements in the literature[32,33] give values of (187 and 188) K, respectively.

Figure 3 shows the deviations of literature data from this work for $[Pyr_{14}][Tf_2N]$. There is, again, excellent agreement with the

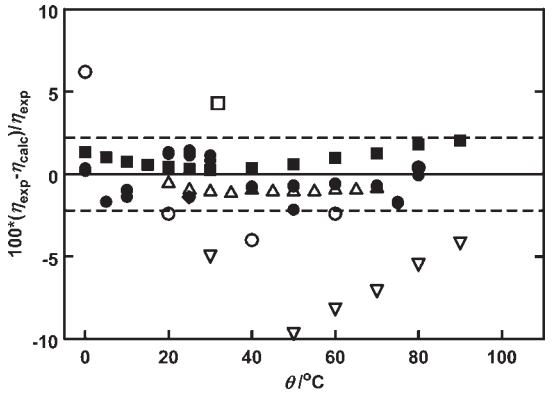

Figure 3. Residuals (experimental−calculated values) for the fit of the experimental viscosities for $[Pyr_{14}][Tf_2N]$ at atmospheric pressure to eq 8 as a function of Celsius temperature, θ. The dashed lines represent the expanded uncertainty of fit (k = 2) or 95 % confidence limits for the fit. Symbols: ●, this work, falling body viscometer; ■, this work, Stabinger viscometer; ○, ref 35, cone−plate viscometer,no uncertainty given; □, ref 36, rotary viscometer, no uncertainty given; Δ, ref 27, capillary viscometer, ± 2 %; ▽, ref 29, Stabinger viscometer, ± 2 %; ♦, ref 34, capillary viscometer, uncertainty not given, estimated at ± 2 % from Table 2 of this reference.

capillary results of Pereiro et al.[27] and with the single capillary point of Pan et al.[29] The rotary viscometer results of Tokuda et al.[35] and of Castiglioni et al.,[36] both of unstated precision, straddle our results. The Stabinger viscometer results of Shamsipur et al.[31] and the cone−plate rheometer results of Comminges et al.[37] (± 1 %) are much lower, possibly due to water contamination.

As in our previous studies, modified Litovitz (ML) and VTF (MVTF1, MVFT2) equations have been used to fit the $[Pyr_{14}]$-$[Tf_2N]$ data set as a whole:

$$\eta = \exp(a + bp + (c + dp + ep^2)/T^3) \quad \text{(ML)} \qquad (10)$$

$$\eta = \exp(a' + b'p + (c' + d'p + e'p^2)/(T - T_0)) \quad \text{(MVFT1)} \qquad (11)$$

and

$$\eta = \exp(a'' + b''p + \delta T_0(p)/(T - T_0(p))),$$
$$T_0(p) = x + yp + zp^2 \quad \text{(MVFT2)} \qquad (12)$$

MVFT1 has a pressure-dependent Angell strength factor (D), whereas MVFT2 has a pressure-dependent T_0. In this case, the deviations for ML at high pressures, though not large, were not random, tending to be positive for high and low temperature

Table 5. $[Pyr_{14}][Tf_2N]$: Coefficients of Best Fit for eqs 10 to 12

	coefficients and standard uncertainties		
	η/mPa·s	$10^{12}\ D_+$/m^2·s^{-1}	$10^{12}\ D_-$/m^2·s^{-1}
	ML, eq 10		
a	−0.2395 ± 0.011	7.4563 ± 0.010	7.4280 ± 0.013
$b\cdot10^3$/MPa^{-1}	2.697 ± 0.26	−1.215 ± 0.31	−4.036 ± 0.30
$c\cdot10^{-6}$/K^3	121.824 ± 0.29	−122.609 ± 0.33	−126.552 ± 0.46
$d\cdot10^{-6}$ /(K^3·MPa^{-1})	0.29498 ± 0.0084	−0.3087 ± 0.010	−0.2191 ± 0.010
e/(K^3·MPa^{-2})	−310.0 ± 64	115.6 ± 21	257.6 ± 17
standard uncertainty of fit	2.1	1.5	1.7
	MVFT1, eq 11		
a'	−1.7507 ± 0.040	9.635 ± 0.17	10.246 ± 0.24
$b'\cdot10^3$/MPa^{-1}	−0.532 ± 0.22	3.578 ± 0.52	−0.575 ± 0.50
c'/K	801.6 ± 11	−1004.0 ± 57	−1241.7 ± 89
d'/(K·MPa^{-1})	1.8275 ± 0.040	−2.395 ± 0.12	−1.858 ± 0.13
$e'\cdot10^3$/(K·MPa^{-2})	−0.899 ± 0.19	0.548 ± 0.10	1.3270 ± 0.091
T_0/K	166.540 ± 0.92	150.57 ± 4.7	134.42 ± 6.6
δ[a]	4.81	−6.67	−9.24
standard uncertainty of fit	1.2	1.5	1.5
	MVFT2, eq 12		
a''	−1.8700 ± 0.034	9.612 ± 0.17	10.332 ± 0.22
$b''\cdot10^3$/MPa^{-1}	3.975 ± 0.13	−0.867 ± 0.38	−3.183 ± 0.38
D	5.1063 ± 0.084	−6.589 ± 0.58	−9.67 ± 1.1
x/K	163.661 ± 0.80	151.227 ± 4.7	131.89 ± 6.3
$y\cdot10^2$/(K·MPa^{-1})	0.108 ± 0.18	0.129 ± 0.47	8.329 ± 0.44
$z\cdot10^5$/(K·MPa^{-2})	−14.011 ± 1.5	−10.815 ± 0.97	−9.932 ± 0.94
standard uncertainty of fit	1.0	1.5	1.5

[a] Angell strength factor.

dx.doi.org/10.1021/je2006049 |J. Chem. Eng. Data 2011, 56, 4672–4685

Table 6. (a) Self-Diffusion Coefficients for P_{14}^+ in [Pyr_{14}][Tf_2N] from θ = (25 to 80) °C and at p = (0.1 to 225) MPa[a], (b) Self-Diffusion Coefficients for Tf_2N^- in [Pyr_{14}][Tf_2N] from θ = (25 to 80) °C and at p = (0.1 to 250) MPa [a], and (c) Self-Diffusion Coefficients for [3-ABN_{13}]-[Tf2N] from θ = (65 to 80) °C and at p = 0.1 MPa[a]

(a)

sealed NMR tube		high pressure cell		
θ/°C	$D_+/10^{-12}m^2\cdot s^{-1}$	θ/°C	p/MPa	$D_+/10^{-12}m^2\cdot s^{-1}$
sample 1		sample 3		
25.00	17.5	20.05	0.1	13.52
25.00	16.6	20.06	0.1	13.53
25.02	17.7	25.03	0.1	17.00
25.06	16.8	25.03	0.1	16.93
30.08	21.4	29.99	0.1	20.92
30.11	21.0	30.06	0.1	21.16
40.14	31.7	30.10	9.5	18.89
40.17	31.4	30.04	10.0	18.76
49.96	44.2	30.05	24.5	15.53
50.02	45.6	30.06	25.0	15.75
50.26	46.4	30.07	37.5	13.42
50.36	46.4	30.07	37.5	13.48
59.78	62.7	30.08	50.0	11.57
59.79	62.8	30.08	50.0	11.45
69.92	83.5	50.09	0.1	45.92
69.98	82.3	50.10	0.1	45.72
74.77	94.1	50.15	0.1	45.97
74.86	92.9	50.10	10.3	40.78
79.68	104	50.10	10.3	40.83
79.73	106	50.10	25.0	35.31
sample 2, dried with Li		50.11	25.0	35.20
29.97	21.4	50.11	48.5	27.62
30.00	21.5	50.10	49.8	27.38
49.97	46.5	50.10	74.2	22.09
50.03	46.0	50.11	74.5	21.93
79.36	110	50.11	99.0	17.69
sample 3		50.10	100.0	17.29
25.05	16.9	50.11	124.3	13.63
25.03	16.7	50.11	125.0	13.44
25.04	16.7	64.91	0.1	72.70
25.06	17.2	64.91	0.1	72.44
30.04	21.8	64.92	0.1	72.11
30.05	21.3	64.91	10.0	66.17
30.05	21.3	64.91	10.0	65.46
30.07	21.1	64.91	24.5	56.87
40.11	32.3	64.92	24.5	57.48
40.20	32.2	64.93	49.5	45.20
40.20	32.5	64.92	50.4	44.81
50.15	31.8	64.93	75.5	36.44
50.36	32.3	64.93	75.5	36.12
75.23	32.1	64.93	100.4	29.45
75.27	44.8	64.94	100.5	29.42
79.97	45.5	64.94	124.6	23.74
80.22	97.4	64.94	125.0	24.43
	96.1	64.94	149.3	19.53

Table 6. Continued

(a)

sealed NMR tube		high pressure cell		
θ/°C	$D_+/10^{-12}m^2\cdot s^{-1}$	θ/°C	p/MPa	$D_+/10^{-12}m^2\cdot s^{-1}$
	109	64.93	150.0	19.05
	109	64.94	174.6	15.50
		64.94	174.8	15.60
		74.91	0.1	92.64
		74.92	0.1	94.72
		74.92	0.1	97.06
		74.91	10.0	85.83
		74.92	10.0	87.97
		74.91	25.0	75.97
		74.92	25.0	77.13
		74.92	49.2	61.73
		74.92	50.0	62.60
		74.92	74.2	50.71
		74.92	75.2	50.78
		74.92	99.8	42.10
		74.92	100.0	41.56
		74.93	124.0	34.92
		74.92	125.0	34.05
		74.92	150.0	28.12
		74.93	150.0	28.26
		74.93	174.5	23.36
		74.93	175.0	23.48
		74.93	199.7	19.43
		74.92	200.0	18.97
		74.92	225.0	15.80
		74.93	225.0	15.86

(b)

sealed NMR tube		high pressure cell		
θ/°C	$D_-/10^{-12}m^2\cdot s^{-1}$	θ/°C	p/MPa	$D_-/10^{-12}m^2\cdot s^{-1}$
sample 1		sample 3		
25.45	14.78	29.71	0.1	17.90
25.51	14.30	29.82	0.1	17.72
30.08	17.78	30.10	0.1	17.32
30.11	17.75	30.07	13.5	14.96
40.09	26.89	30.09	13.6	15.21
40.10	26.95	28.90	25.0	12.95
49.99	38.95	29.68	25.0	13.08
50.00	39.27	29.17	50.8	10.21
50.03	38.58	29.72	50.8	10.13
50.06	39.72	29.98	75.5	7.66
59.97	53.63	30.05	75.5	7.78
59.98	53.38	50.12	0.1	39.76
70.11	74.23	50.13	0.1	39.66
70.13	72.75	50.14	12.0	35.42
74.97	84.28	50.15	12.5	34.31
75.02	85.45	50.16	24.5	30.90
80.17	96.10	50.16	24.5	30.75
80.17	95.94	50.18	50.0	23.82
sample 2, dried over Li		50.18	50.0	23.53
25.03	14.91	50.20	74.5	18.81

dx.doi.org/10.1021/je2006049 |J. Chem. Eng. Data 2011, 56, 4672–4685

Table 6. Continued

(b)				
sealed NMR tube		high pressure cell		
θ/°C	$D_-/10^{-12}m^2 \cdot s^{-1}$	θ/°C	p/MPa	$D_-/10^{-12}m^2 \cdot s^{-1}$
25.03	14.73	50.19	75.0	18.28
40.16	27.53	50.19	99.0	14.99
40.16	27.43	50.22	100.0	14.67
50.06	39.46	50.23	124.2	12.18
69.97	74.38	50.23	124.4	12.05
79.66	97.35	64.79	0.1	63.94
		64.95	0.1	63.79
		64.96	0.1	62.77
		65.03	0.1	65.24
		65.17	0.1	64.34
		64.97	9.3	57.11
		64.98	10.5	56.70
		65.06	24.3	50.11
		65.09	25.4	49.62
		65.10	48.0	40.12
		65.10	50.4	39.52
		65.11	74.0	32.38
		65.10	75.0	31.56
		64.86	97.5	26.53
		65.11	99.0	25.95
		64.94	124.0	21.13
		64.81	124.3	21.36
		65.25	147.5	17.50
		65.06	149.4	17.50
		65.07	149.4	17.32
		65.18	174.5	14.65
		65.18	175.0	14.35
		65.20	198.5	12.03
		65.20	200.5	12.03
		74.40	0.1	83.37
		74.60	0.1	83.93
		75.02	0.1	81.42
		75.23	0.1	82.94
		75.32	0.1	84.57
		75.34	0.1	84.70
		74.62	12.5	75.52
		74.71	12.5	74.07
		74.82	25.0	67.03
		74.90	25.0	68.68
		74.92	50.2	54.75
		74.92	50.2	53.60
		74.94	73.0	44.33
		74.97	75.0	44.37
		75.34	75.0	43.72
		75.03	98.0	36.00
		75.31	101.0	35.26
		75.08	105.0	35.03
		75.31	124.3	29.81
		75.31	124.3	29.50
		75.31	149.4	24.23
		75.30	150.3	24.27
		75.29	174.5	20.43

Table 6. Continued

(b)				
sealed NMR tube		high pressure cell		
θ/°C	$D_-/10^{-12}m^2 \cdot s^{-1}$	θ/°C	p/MPa	$D_-/10^{-12}m^2 \cdot s^{-1}$
		75.31	174.5	20.17
		75.26	200.0	17.24
		75.27	200.0	16.90
		75.25	224.5	14.40
		75.27	225.0	14.49
		75.29	250.0	12.44
		75.30	250.0	12.41

(c)			
θ/°C	$D_+/10^{-12}m^2 \cdot s^{-1}$	T/°C	$D_-/10^{-12}m^2 \cdot s^{-1}$
64.82	17.33	64.85	18.77
64.87	17.70	64.88	18.82
69.69	21.23	70.03	23.37
69.77	21.25	70.10	23.16
74.69	26.34	74.98	28.33
74.74	26.08	75.01	29.05
79.73	32.84	79.67	33.40
79.81	32.49	79.80	33.43

[a] Standard uncertainties u are $u(T) = 0.02$ K, $u(p) = 0.2$ MPa above 1 MPa and $u(D) = 3$ %.

isotherms, and negative between, whereas the more temperature-flexible MVFT equations gave quite good fits. A better fit (± 1.5 %) is obtained if the temperature exponent in eq 10 is allowed to float, giving 3.24 instead of the Litovitz value of 3. This poorer fit to ML than for the atmospheric pressure analogue [eq 7] may be due to the effects of supercooling under pressure as $[Pyr_{14}][Tf_2N]$ freezes at −8.65 °C at 0.1 MPa.[38] However the $T-p$ freezing line has yet to be determined. The coefficients for eq 10 to 12 are given in Table 5. There appear to be no previously published high-pressure viscosity measurements for $[Pyr_{14}][Tf_2N]$.

c. Self-Diffusion Coefficients. Ion self-diffusion coefficients for both compounds are listed in Table 6, including high pressure measurements for $[Pyr_{14}][Tf_2N]$. They were fitted to the analogues of eqs 7, 8, and 10 to 12 and the coefficients are given in Tables 4 and 5. For $[Pyr_{14}][Tf_2N]$ at atmospheric pressure, there is good agreement with the results of Tokuda et al.,[35] (as represented by their VFT equation), with a mean bias of (3.0 and 1.2) % for D_+ and D_-, respectively. The values for D_+ and D_- at 32 °C of Castiglioni et al.[36] are 9 and 3 % higher than those of this work, and the single point for D_+ of Annat et al.[39] at 20 °C is 4 % higher. Though measurements were made by Castiglioni et al. at other temperatures, regrettably, no numerical values are given. There are no published diffusion measurements for $[3\text{-}ABN_{13}][Tf_2N]$.

d. Conductivity. Conductivity values for $[Pyr_{14}][Tf_2N]$ at atmospheric pressure are listed in Table 7. They were fitted to the analogues of eqs 7 and 8, and the coefficients are also given in Table 4. The fit to the VFT equation is much the superior. Previous measurements have been made by Salminen et al.,[32](reported in graphical form only), Tokuda et al.[35] (VFT equation), Castiglione et al.[36] [only a single point is recorded, for 305 K, though measurements were said to have been carried out from (−40 to +100) °C] and Martinelli et al.[40] (reported in graphical

Table 7. Conductivity κ and Molar Conductivity Λ of $[Pyr_{14}][Tf_2N]$ from θ = (0 to 80) °C[a]

θ/°C	κ/S·m^{-1}	Λ/μS·m^2·mol^{-1}
0.00	0.07415	22.11
5.00	0.1012	30.26
10.00	0.1343	40.30
15.00	0.1745	52.51
19.99	0.2212	66.78
24.99	0.2755	83.45
25.00	0.2754	83.42
30.00	0.3379	102.7
40.00	0.4864	148.7
49.99	0.6674	205.4
60.00	0.8788	272.2
69.99	1.122	349.5
80.00	1.392	436.7

[a] Standard uncertainties u are $u(T) = 0.01$ K, $u(\kappa) = 2$ % and $u(\Lambda) = 2$ %.

form only). A numerical value seemingly derived from ref 40 is cited by Johansson et al.[41] for 20 °C. The results of Tokuda et al.[35] agree quite well with those of this work, with standard and maximum deviations of (1 and 2) % respectively in the region of overlap. The values given by Castiglione et al.[36] and Johansson et al.[41] are lower by (24 and 19) %, respectively.

No measurements were made for $[3\text{-}ABN_{13}][Tf_2N]$ as insufficient material was available.

DISCUSSION

In our earlier work on the inter-relation of the transport properties of ionic liquids we have employed the Stokes−Einstein and Nernst−Einstein equations and computed velocity correlation coefficients.[3,7,42] Here we continue these approaches for $[Pyr_{14}][Tf_2N]$, and also examine the application of thermodynamic or density scaling.[17] This type of scaling reduces transport property isotherms to a smoothed function of the temperature-molar volume group (TV^{γ}), where γ is a fitted constant. It was originally employed for the analysis of dielectric relaxation times of glassy polymers,[43] and has been applied to the viscosity of ionic liquids by Roland et al.[17] and Pensado et al.[18] In further work by the Fernández group,[19] such scaling has been extended to diffusion coefficients and electrical conductivities. γ can be related to the Grüneisen constant[44] and, for the model inverse power law liquid, is equal to $(n/3)$ where n is the repulsive exponent.[17,44] A detailed analysis of the theory and the interpretation of γ for van der Waals liquids has been given by Schrøder et al.[45]

Stokes−Einstein Relation. In earlier studies of 1-*n*-alkyl-3-methylimidazolium tetraborates and hexafluorophosphates, we fitted our results to fractional forms of the Stokes−Einstein and Walden relations:[3,7]

$$\Lambda T \propto D \propto \left(\frac{T}{\eta}\right)^{s} \tag{13}$$

In this we followed Voronel et al.,[46] who plotted log(resistivity) versus log(viscosity) plots [i.e., $\ln(r/T)$ against $\ln(\eta/T)$] for inorganic molten salts such as $Ca_2K_3(NO_3)_7$, neglecting the temperature-dependent concentration (density) term contained in Λ. (This temperature dependence is small relative to the change in the conductivity in their examples.) Subsequent work on the Lennard-Jones fluid where simulation results are available over very broad ranges of temperature and density, and an examination of high-pressure experimental data for both (non-hydrogen bonded) molecular and ionic liquids,[47] suggests that the classical forms are to be preferred, that is:

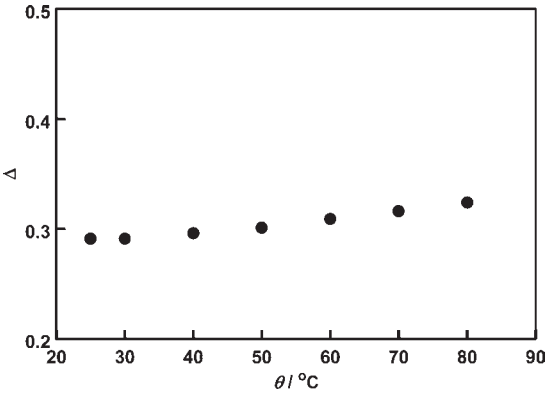

Figure 4. Nernst−Einstein deviation factor for $[Pyr_{14}][Tf_2N]$, Δ, at 0.1 MPa.

$$\Lambda \propto \frac{D}{T} \propto \left(\frac{1}{\eta}\right)^{t} \tag{14}$$

Thus it is possible to collapse isotherms and isobars, i.e., all state points, onto a single curve given by the scaling exponent, t. For the imidazolium salts, fitted values of t are indistinguishable from those for s, (0.90 ± 0.05), very probably because the temperature range for the available data is relatively short.[47] Nevertheless, eq 14 is a good consistency test for experimental results. For $[Pyr_{14}][Tf_2N]$, the fit to $D_+(T,p)$ is t = (0.94 ± 0.05) and for $D_-(T,p)$ is (0.93 ± 0.05). For the (atmospheric pressure) molar conductivity, $\Lambda(T)$, t = (0.93 ± 0.05).

Nernst−Einstein Equation. The Nernst−Einstein equation linking the molar conductivity with the ion self-diffusion coefficients can be written[3,7,42,47] as

$$\Lambda = \frac{F^2}{RT}(\nu_+ z_+^{\,2} D_+ + \nu_- z_-^{\,2} D_-)(1 - \Delta) \tag{15}$$

where ν_i and z_i are stoichiometric and charge numbers respectively for a salt formally dissociating as

$$A_{\nu+}B_{\nu-} \rightleftharpoons \nu_+ A^{z+} + \nu_- B^{z-} \tag{16}$$

R and F are the gas and Faraday constants, T is the temperature, and Δ is the NE deviation parameter.

As we only have conductivity data for atmospheric pressure, the following discussion is constrained to this condition. A plot of $\ln(T\Lambda)$ against $\ln(D_+ + D_-)$ has a slope of (0.99 ± 0.05), so there is very good consistency between the cationic and anionic diffusion coefficients, and the conductivity data. A constant slope in this plot implies a constant Δ: our data yield (0.313 ± 0.013) for the range defined by the diffusion data, (25 to 80) °C, slightly increasing with increasing temperature (Figure 4). This is a lower value than those obtained for the 1-*n*-alkyl-3-methylimidazolium tetraborates and hexafluorophosphates, where Δ ranged from 0.37 to 0.52,[3,7] or for $[BMIM][Tf_2N]$, Δ = 0.37.[48] The lack of any definite dependence on temperature for Δ ($[Pyr_{14}][Tf_2N]$) is consistent with the results for the imidazolium salts. By contrast, Hayamizu et al.[49] have reported a strongly temperature

Table 8. VCC (f_{ij}) and Nernst−Einstein Δ for $[Pyr_{14}][Tf_2N]$ from θ = (0 to 80) °C

θ/°C	c/mol·dm^{-3}	ϕ/(Pa·s)$^{-1}$	f_{++}[a]	f_{--}	f_{+-}	Δ
0.0	3.354	3.16			−0.359	
5.0	3.344	4.39			−0.502	
10.0	3.333	5.93			−0.683	
15.0	3.322	7.84			−0.909	
20.0	3.312	10.2			−1.18	
25.0	3.301	12.9	−2.18	−3.59	−1.50	0.291
30.0	3.291	16.1	−2.74	−4.51	−1.89	0.291
40.0	3.270	24.1	−4.17	−6.86	−2.84	0.296
50.0	3.249	34.3	−6.03	−9.98	−4.07	0.301
60.0	3.229	46.9	−8.40	−14.02	−5.60	0.309
70.0	3.210	62.0	−11.28	−19.08	−7.46	0.316
80.0	3.188	79.6	−14.72	−25.28	−9.65	0.324

[a] Units: $10^{-15}m^5 \cdot mol^{-1} \cdot s^{-1}$.

dependent Δ for the closely related salt, $[Pyr_{13}][Tf_2N]$, which differs from $[Pyr_{14}][Tf_2N]$ only in having an propyl radical on the N-atom of the cation instead of a butyl radical, (Δ ∼ 0.3 to 0.5, (10 to 80) °C, smaller at lower temperature).[50,49] This seems to be an anomaly, but similar behavior is also reported by the Hayamizu group for $[Pyr_{13}]$ bis(fluorosulfonyl)amide,[49] tri*n*-ethylpentylphosphonium$[Tf_2N]$ and the substituted ammonium analogue of the latter IL.[52] Hayamizu et al.[49] noted a rather large difference between the FSE slope for ionic diffusion ($t \sim 1$) and the Walden-plot slope for Λ, ($t \sim 0.78$), which is also unusual, so further investigation is warranted.

Velocity Correlation Coefficients. The velocity cross-correlation coefficients (VCC or f_{ij}), defined by Schönert (for the mass-fixed frame of reference), connect the conductivity and ion diffusion coefficients[53]

$$f_{++} \equiv \frac{N_A V}{3}\int_0^\infty \langle v_{+\alpha}(0)v_{+\beta}(t)\rangle \, dt = RT\kappa\left(\frac{M_-}{z_- FcM}\right)^2 - \frac{D_+}{\nu_+ c} \quad (17)$$

$$f_{--} \equiv \frac{N_A V}{3}\int_0^\infty \langle v_{-\alpha}(0)v_{-\beta}(t)\rangle \, dt = RT\kappa\left(\frac{M_+}{z_+ FcM}\right)^2 - \frac{D_-}{\nu_- c} \quad (18)$$

and

$$f_{+-} \equiv \frac{N_A V}{3}\int_0^\infty \langle v_{+\alpha}(0)v_{-\beta}(t)\rangle \, dt = RT\kappa\frac{M_+ M_-}{z_+ z_- (FcM)^2} \quad (19)$$

where N_A is the Avogadro constant, V is the volume of the ensemble, κ is the conductivity, c is the amount concentration (molarity) of salt, and M, M_+, and M_- are the molar masses of salt, cation, and anion, respectively. It is the differences between these that define the value of Δ in the Nernst−Einstein relation,

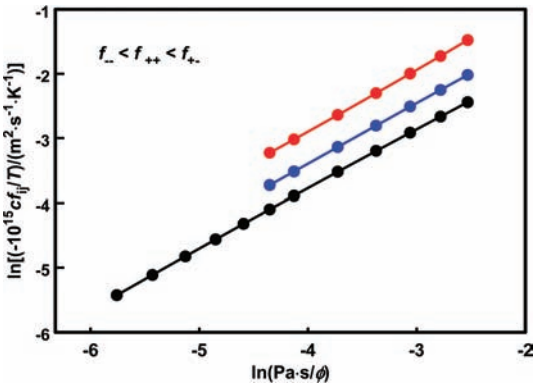

Figure 5. Plot of $\ln[(-cf_{ij}/T)/(10^{-15}m^2 \cdot s^{-1} \cdot K^{-1})]$ versus $\ln[(Pa \cdot s)/\phi]$ for $[Pyr_{14}][Tf_2N]$. The f_{ij} are velocity cross-correlation coefficients, and ϕ is the fluidity or reciprocal viscosity. This is analogous to a Stokes−Einstein plot of $\ln(D_i/T)$ or a Walden plot of ln Λ against ln ϕ. Symbols: blue, f_{++}; red, f_{--}; black, f_{+-}. Contrast the reversed relative positions of the cation−cation and anion−anion lines to those for $[BMIM][BF_4]$ in ref 42 Figure 2. The slopes are 0.96, 0.94, and 0.92_5 for f_{--}, f_{++}, and f_{+-} respectively.

eq 14[3,7,42,47]

$$\Delta = -\frac{c(2\nu_+\nu_- z_+ z_- f_{+-} + \nu_+^2 z_+^2 f_{++} + \nu_-^2 z_-^2 f_{--})}{(\nu_+ z_+^2 D_+ + \nu_- z_-^2 D_-)} = -\frac{c(f_{++} + f_{--} - 2f_{+-})}{(D_+/\nu_+ + D_-/\nu_-)} \quad (20)$$

or, for a 1:1 salt

$$\Delta = \frac{c(2f_{+-} - f_{++} - f_{--})}{(D_+ + D_-)} \quad (21)$$

While nonzero values of Δ are sometimes attributed to ion-association of some type that might reduce charge mobility relative to ion diffusive mobilities, it has been shown as long ago as the 1960s[55] that due to momentum transfer there is a distortion of the symmetry of the surroundings of a given ion. Hence an internal electric field acts on a given ion antiparallel to any applied external field. Hence the charge mobility in this reduced field is less than the diffusive mobility.

Values of the VCC are given in Table 8. In contrast to the behavior of 1-methyl-3-alkylimidazolium BF_4 and PF_6 salts, it was earlier found for a number of Tf_2N^- salts that $f_{--} < f_{++}$.[56] The results for $[Pyr_{14}][Tf_2N]$ are consistent with this finding. As yet velocity cross-correlation functions (but not the coefficients) have been computed by molecular dynamics simulations for only a single ionic liquid, $bmimPF_6$.[57] While interesting effects are found showing momentum transfer between primary and secondary ion co-ordination shells for the two models employed, D_+ is predicted to be less than D_-, contrary to experiment.[3]

The VCC show regularities, in that when plotted against the reciprocal viscosity, or fluidity, values obtained at different state points scale onto common curves.[3,7,42,47] This has been shown to be a consequence of the (fractional) Stokes−Einstein relation.[42,47] From eq 19, the group $(z_+z_-cf_{+-}/T)$ depends on the viscosity in the same way as Λ (= κ/c). Thus a graph of $\ln(z_+z_-cf_{+-}/T)$ versus $\ln(\eta)$ is really a Walden plot. Given the similarity of the fractional Stokes−Einstein equation parameters, t, for the ion-self-diffusion coefficients, the same scaling also applies to the two other f_{ij}. The result is shown in Figure 5, where

Table 9. Thermodynamic Scaling Parameters for $[Pyr_{14}][Tf_2N]$

property	γ	ϕ	st. devn/%
Casalini−Roland (Avramov) Model, eqs 21 and 22			
η	3.06 ± 0.03	2.16 ± 0.03	2.4
D_+	3.12 ± 0.02	1.92 ± 0.07	2.0
D_-	3.05 ± 0.02	1.46 ± 0.07	2.2
Scaling to Polynomial in (TV^{γ})			
η^a	3.00 ± 0.05		2.3
$D_+{}^b$	3.10 ± 0.05		2.1
$D_-{}^b$	3.00 ± 0.05		1.6
Scaling of Reduced Variables (eqs 25 and 26) to Polynomial in (TV^{γ})			
η^a	2.80 ± 0.05		2.0
$D_+{}^b$	3.20 ± 0.05		0.7
$D_-{}^b$	3.17 ± 0.05		2.0

[a] Quartic. [b] Binomial.

the functions $\ln(-cf_{ij}/T)$ are plotted against $\ln(1/\eta)$ for the three VCC (the z_i in eq 17 to 19 are signed). (Note that the quantities (cf_{ij}) are the "distinct" diffusion coefficients introduced by Friedman and Mills.[58]) The three lines have similar slopes, as is found for other ionic liquids.

Scaling. As mentioned above, it has been found that the viscosity, dielectric relaxation times and self-diffusion coefficients of molecular liquids can be scaled in terms of the group (TV^{γ}) where γ is a constant for a given liquid.[17−19,43−45] For a model inverse power law (IPL) fluid, the scaling is exact, with $\gamma = n/3$, n being the power of the repulsive intermolecular potential.[17,44,45] For model fluids having attractive terms, such as the Lennard-Jones, and real liquids, the values of γ obtained from scaling of the transport properties are affected by the attractive forces, that is the scaling is to an effective IPL: for instance, $\gamma > n/3$ for Lennard-Jones fluids[59] and high values of γ are generally found for molecular fluids without specific interactions such as H-bonding.[17−19,44] It has been argued by Schrøder et al.[45] that scaling should not necessarily apply to ionic liquids as the interaction potential includes Coulombic terms, not just van der Waals repulsions and attractions. However empirical fits for ionic liquids do appear to work,[17−19] (though no tests have yet been made for high-temperature molten salts), and thermodynamic scaling may provide a convenient way of fitting high-pressure transport property data to temperature and density using relatively few coefficients if suitable functional(s) of (TV^{γ}) can be found.

Though most authors appear to have used empirical[17,44] or graphical[17,60] fits, a stretched exponential form has been derived by Casalini et al.,[44] based on a modification of the Avramov model for glass-transition dynamics. This method uses two fitted parameters, γ and ϕ, but these are not independent.[18,60] For the viscosity[17,18] and self-diffusion coefficients[19] the expressions are

$$\eta(T,V) = \eta_0 \exp\left[\left(\frac{A_\eta}{TV^{\gamma_\eta}}\right)^{\phi_\eta}\right] \quad (22)$$

$$D(T,V) = D_0 \exp\left[-\left(\frac{A_D}{TV^{\gamma_D}}\right)^{\phi_D}\right] \quad (23)$$

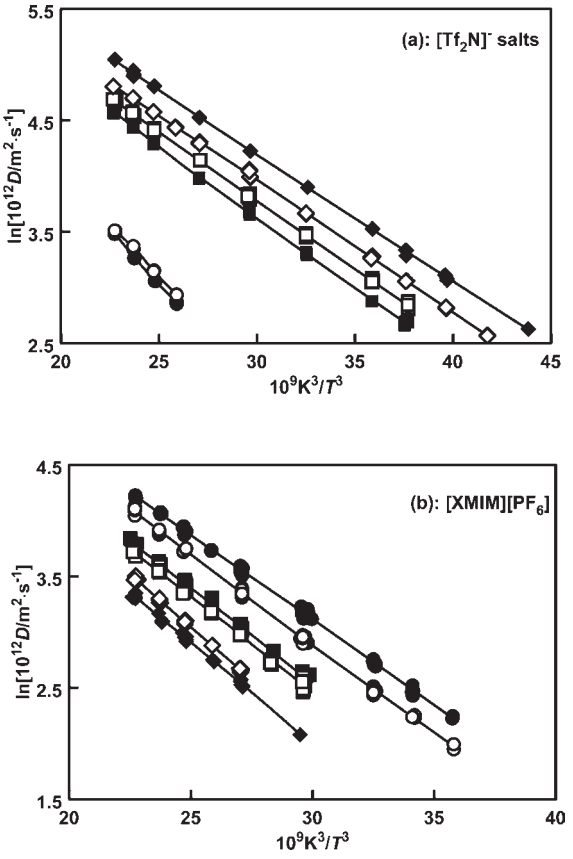

Figure 6. (a) Litovitz plot of the ion self-diffusion coefficients of [BMIM][Tf_2N], diamonds, [Pyr_{14}][Tf_2N], squares, and [3-ABN_{13}]-[Tf_2N], circles. Closed symbols are for cations and open ones for anions. The molar volumes at 25 °C are 291.9, 302.9, and 329.3 $cm^3 \cdot mol^{-1}$, respectively. (b) Litovitz plot of the ion self-diffusion coefficients of [BMIM][PF_6], circles, [HMIM][PF_6], squares, and [OMIM][PF_6], diamonds. Closed symbols are for cations and open ones for anions. The molar volumes at 25 °C are 207.8, 241.4, and 275.1 $cm^3 \cdot mol^{-1}$, respectively.

Good fits to these equations have been obtained by Lopez et al.[19] for a number of ionic liquids based on substituted imidazolium cations. Values of the fitted parameters for [Pyr_{14}][Tf_2N] are given in Table 9: consistent γ and ϕ parameters are found for the three properties, the values for γ being similar to those obtaining for the imidazolium ionic liquids and molten tetra-alkyl ammonium salts examined by Lopez et al.[19] (1.83 to 3.54).

An alternative is to fit the data, expressed as ln η or ln D, to simple (2nd or 3rd order) polynomials in (TV^{γ}).[42,61] This procedure yielded very similar γ values to those obtained from the Casalini−Roland stretched exponential equations (Table 9).

All of these values are lower than those generally found for simple molecular liquids (from 6 to 15), but of similar order to those obtained for longer chain molecules and large esters where the larger dispersion forces seem to influence the values of γ.

Gnan et al.[62] define "isomorphous" thermodynamic states as those for which the potential energy scales as

$$\exp(-U_1/kT_1) = C_{12} \exp(-U_2/kT_2) \quad (24)$$

For an IPL liquid, the constant C_{12} is unity. They state that for isomorphic states, the transport properties are invariant when reduced units are employed. For the viscosity and self-diffusion

coefficient the appropriate expressions are

$$\tilde{\eta} = \eta v^{2/3}/\sqrt{mkT} \quad (25)$$

$$\tilde{D} = Dv^{-1/3}\sqrt{m/kT} \quad (26)$$

where m is the molecular mass and v the molecular volume.[62] Fragiadakis and Roland,[60] using graphical methods, have shown that for a number of molecular liquids, where relatively narrow ranges of the viscosity or the self-diffusion coefficient are available, the values of γ derived from these two properties are much closer together than those derived from unreduced physical quantities. For their best example, cyclohexane, γ derived from the viscosity goes from 11 to 7.5, and that derived from the self-diffusion coefficient goes from 6 to 7.5. On the other hand, for materials such as squalane, where viscosity data are available over several orders of magnitude, reduction hardly changes the value of γ as T and V vary much less, proportionately. Lopez et al.[19] have checked the effect of reduction for imidazolium ionic liquids and molten tetra-alkyl ammonium salts, with the assumption that the salt molar volume can be used in the expressions for the ion self-diffusion coefficients, but found only slight change, though γ for the viscosity does tend to decrease and that for a self-diffusion coefficient to increase, in accord with the pattern shown by molecular liquids. Here, the $[Pyr_{14}][Tf_2N]$ γ values are hardly changed for the reduced quantities, $\tilde{\eta}$, $\tilde{D}_+$, and $\tilde{D}_-$ (Table 9).

Structure-Diffusion Coefficient Relationships. A lesser aim of this work was to examine the effect of the replacement of the puckered pyrrolidinium ring by the larger bicyclic azenonaneium structure. Figure 6a compares Litovitz plots of the ion self-diffusion coefficients of $[Pyr_{14}][Tf_2N]$ and $[3\text{-}ABN_{13}][Tf_2N]$, and $[BMIM][Tf_2N]$,[48] which has a flat ring structure for the cation. At a fixed temperature, the self-diffusion coefficients decrease with increasing salt molar volume, but the ratio of D(cation) to D(anion) changes from values greater than unity to less than unity. These effects are similar to those seen, for example, in 1-alkyl-3-methylimidazolium PF_6^- salts as the alkyl chain is made longer,[3,7] shown in Figure 6b, and appear to be general for ionic liquids series with common anions.

CONCLUSIONS

The viscosities and ion self-diffusion coefficients of the ionic liquid $[Pyr_{14}][Tf_2N]$ are reported between (0 and 90) °C and at pressures to 103 MPa and between (25 and 80) °C and at pressures to 250 MPa, respectively. Conductivities and densities obtained between (0 and 90) °C at atmospheric pressure are also reported. Ion self-diffusion coefficients and densities, obtained at atmospheric pressure, are also given for *N*-methyl-*N*-propyl-3-azabicyclo[3.2.2]nonaneium bis(trifluoromethylsulfonyl)amide.

The temperature derivative of the thermal expansivity of $[3\text{-}ABN_{13}]$ $[Tf_2N]$ is found to be slightly negative, whereas that for $[Pyr_{14}][Tf_2N]$ is close to zero.

The diffusion and viscosity data were fitted to the Litovitz and VFT equations, using the (now standard) high pressure forms for $[Pyr_{14}][Tf_2N]$.

The fractional Stokes−Einstein relation is found to apply to $[Pyr_{14}][Tf_2N]$. The exponent t is (0.94 ± 0.05) for the cation and (0.93 ± 0.05) for the anion. For the fractional Walden relation, t = (0.93 ± 0.05). A plot of $\ln(T\Lambda)$ against $\ln(D_+ + D_-)$ has a slope of (0.99 ± 0.05), so there is very good consistency between the cationic and anionic diffusion coefficients, and the conductivity data. The Nernst−Einstein deviation parameter, Δ, is (0.313 ± 0.013). This is consistent with the following inequality for the ion−ion velocity cross-correlation coefficients: $f_{+-} > (f_{++} + f_{--})/2$. For $[Pyr_{14}][Tf_2N]$, $f_{--} < f_{++} < f_{+-}$, concordant with results for other $[Tf_2N]^-$ salts but contrasting with $[BF_4]^-$ and $[PF_6]^-$ salts where $f_{++} < f_{--} < f_{+-}$. The VCC show regularities, in that when plotted against the reciprocal viscosity, values obtained at different state points scale onto common curves. When plotted in an analogue of the fractional Stokes−Einstein relation in the form of distinct diffusion coefficients, similar slopes are obtained for the cation−cation, anion−anion, and cation−anion interactions.

Thermodynamic scaling has been applied to both unreduced and reduced viscosities and ion self-diffusion coefficients for $[Pyr_{14}][Tf_2N]$. Consistent γ values are obtained for η, D_+ and D_-, treated with the Casalini-Roland model and with a simple polynomial fit in (TV^{γ}), and for the reduced quantities, $\tilde{\eta}$, $\tilde{D}_+$, and $\tilde{D}_-$.

At a fixed temperature, the self-diffusion coefficients for the series $[BMIM][Tf_2N]$, $[Pyr_{14}][Tf_2N]$, and $[3\text{-}ABN_{13}][Tf_2N]$ decrease with increasing salt molar volume, but the ratio of D(cation) to D(anion) changes from values greater than unity to less than unity, in common with what is generally observed for ionic liquid series.

AUTHOR INFORMATION

Corresponding Author

*E-mail: k.harris@adfa.edu.au.

Funding Sources

K.R.H. is grateful to CSIRO Energy Technology and the Research Fund of the Royal Society of Chemistry for financial support for this work.

ACKNOWLEDGMENT

It is a pleasure to thank Miss Eriko Niitsuma (Sendai) for her assistance with the conductivity and DSC experimental measurements.

REFERENCES

(1) Harris, K. R.; Woolf, L. A.; Kanakubo, M. Temperature and Pressure Dependence of the Viscosity of the Ionic Liquid 1-Butyl-3-methylimidazolium Hexafluorophosphate. *J. Chem. Eng. Data* **2005**, *50*, 1777–1782.

(2) Harris, K. R.; Woolf, L. A.; Kanakubo, M. Temperature and Pressure Dependence of the Viscosity of the Ionic Liquids 1-Octyl-3-methylimidazolium Hexafluorophosphate and 1-Octyl-3-methylimidazolium Tetrafluoroborate. *J. Chem. Eng. Data* **2006**, *51*, 1161–1167.

(3) Kanakubo, M.; Harris, K. R.; Tsuchihashi, N.; Ibuki, K.; Ueno, M. Effect of Pressure on Transport Properties of the Ionic Liquid 1-Butyl-3-methylimidazolium Hexafluorophosphate. *J. Phys. Chem. B* **2007**, *111*, 2062–2069.correction, **2007**, *111*, 13867.

(4) Kanakubo, M.; Harris, K. R.; Tsuchihashi, N.; Ibuki, K.; Ueno, M. Temperature and Pressure Dependence of the Electrical Conductivity of the Ionic Liquids 1-Methyl-3-octylimidazolium Hexafluorophosphate and 1-Methyl-3-Octylimidazolium Tetrafluoroborate. *Fluid Phase Equilib.* **2007**, *261*, 414–420.

(5) Harris, K. R.; Woolf, L. A.; Kanakubo, M. Temperature and Pressure Dependence of the Viscosity of the Ionic Liquids 1-Hexyl-3-methylimidazolium Hexafluorophosphate and 1-Butyl-3-Methylimidazolium Bis(trifluorosulfonyl)imide. *J. Chem. Eng. Data* **2007**, *52*, 1080–1085.

(6) Harris, K. R.; Woolf, L. A.; Kanakubo, M. Temperature and Pressure Dependence of the Viscosity of the Ionic Liquid 1-Butyl-3-methylimidazolium Tetrafluoroborate: Viscosity and Density Relationships in Ionic Liquids. *J. Chem. Eng. Data* **2007**, *52*, 2425–2430. Correction, **2008**, *53*, 1230.

(7) Harris, K. R.; Kanakubo, M.; Tsuchihashi, N.; Ibuki, K.; Ueno, M. Effect of Pressure on the Transport Properties of Ionic liquids: 1-Alkyl-3-methylimidazolium salts. *J. Phys. Chem. B* **2008**, *112*, 9830–9840.

(8) The anion bis(trifluoromethanesulfonyl)amide or 1,1,1-trifluoro-*N*-[(trifluoromethyl) sulfonylmethanesulfonamide (CAS No. 98837−98−0) is sometimes called bis(trifluoromethanesulfonyl)imide in the literature, as in ref 5. See Wilson, G. J.; Hollenkamp, A. F.; Pandolfo, A. G. Resolving Ambiguous Naming for an Ionic Liquid Anion. *Chem. Int.* **2007**, *29*, 16–18.

(9) MacFarlane, D. R.; Meakin, P.; Sun, J.; Amini, N.; Forsyth, M. Pyrrolidinium Amides: a New Family of Molten Salts and Conductive Plastic Crystal Phases. *J. Phys. Chem. B* **1999**, *103*, 4164–4170.

(10) Rocher, N. M.; Izgorodina, E. I.; Rüther, T.; Forsyth, M.; MacFarlane, D. R.; Rodopoulos, T.; Horne, M. D.; Bond, A. M. Aluminium Speciation in 1-Butyl-1-Methylpyrrolidinium Bis(trifluoromethylsulfonyl)amide/$AlCl_3$ Mixtures. *Chem.—Eur. J.* **2009**, *15*, 3435–3447.

(11) Rodopoulos, T.; Smith, L.; Horne, M. D.; Rüther, T. Speciation of Aluminium in Mixtures of the Ionic Liquids $[C_3mpip][NTf_2]$ and $[C_4mpyr][NTf_2]$ with $AlCl_3$: An Electrochemical and NMR Spectroscopy Study. *Chem.—Eur. J.* **2010**, *16*, 3815–3826.

(12) Howlett, P. C.; MacFarlane, D. R; Hollenkamp, A. F. High lithium metal cycling efficiency in a room-temperature ionic liquid. *Electrochem. Solid Sate Lett.* **2004**, *7*, A97–A101.

(13) Saint, J.; Best, A. S.; Hollenkamp, A. F.; Kerr, J.; Shin, J.-H.; Doeff, M. M. Compatibility of $Li_xTi_yMn_{1-y}O_2$ (y = 0, 0.11) Electrode Materials with Pyrrolidinium-Based Ionic Liquid Electrolyte Systems. *J. Electrochem. Soc.* **2008**, *155*, A172–A180.

(14) Gardas, R. L.; Costa, H. F.; Freire, M. G.; Carvalho, P. J.; Marrucho, I. M.; Fonseca, I. M. A.; Ferreira, A. G. M.; Coutinho, J. A. P. Densities and Derived Thermodynamic Properties of Imidazolium-, Pyridinium-, Pyrrolidinium-, and Piperidinium-Based Ionic Liquids. *J. Chem. Eng. Data* **2008**, *53*, 805–811.

(15) Jacquemin, J.; Nancarrow, P.; Rooney, D. W.; Costa Gomes, M. F.; Husson, P.; Majer, V.; Pádua, A. A. H.; Hardacre, C. Prediction of Ionic Liquid Properties. II. Volumetric Properties as a Function of Temperature and Pressure. *J. Chem. Eng. Data* **2008**, *53*, 2133–2143.

(16) Rüther, T.; Huang, J.; Hollenkamp, A. F. A New Family of Ionic Liquids Based on N,N-dialkyl-3-azabicyclo[3.2.2]nonanium Cations: Organic Plastic Crystal Behaviour and Highly Reversible Lithium Metal Electrodeposition. *Chem. Commun.* **2007**, 5226–5228.

(17) Roland, C. M.; Bair, S.; Casalini, R. Thermodynamic Scaling of the Viscosity of Van der Waals, H-bonded and Ionic Liquids. *J. Chem. Phys.* **2006**, *125*, 124508−1–124508−8.

(18) Pensado, A. S.; Pádua, A. A. H.; Comuñas, M. J. P.; Fernández, J. Relationship between Viscosity Coefficients and Volumetric Properties Using a Scaling Concept for Molecular and Ionic Liquids. *J. Phys. Chem. B* **2008**, *112*, 5563−-5574.

(19) López, E. R.; Pensado, A. S.; Comuñas, M. J. P.; Pádua, A. A. H.; Fernández, J.; Harris, K. R. Density Scaling of the Transport Properties of Molecular and Ionic Liquids. *J. Chem. Phys.* **2011**, 144507−1–144507−11.

(20) Rüther, T.; Ross, T.; Mensforth, E. J.; Hollenkamp, A. F. N-alkylation of N-heterocyclic Ionic Liquid Precursors in Ionic Liquids. *Green Chem.* **2009**, *11*, 804–809.

(21) Harris, K. R.; Mills, R.; Back, P. J.; Webster, D. S. An Improved NMR Spin-Echo Apparatus for the Measurement of Self-Diffusion Coefficients: the Diffusion of Water in Aqueous Electrolyte Solutions. *J. Magn. Reson.* **1978**, *29*, 473–482.

(22) Harris, K. R. The Density Dependence of the Self-diffusion Coefficient of Chlorotrifluoromethane near the Critical Temperature. *Physica* **1978**, *93A*, 593–610.

(23) Harris, K. R.; Lam, H.-N.; Raedt, R.; Easteal, A. J.; Price, W. E.; Woolf, L. A. The Temperature and Density Dependences of the Self-diffusion Coefficient and the Shear Viscosity of Liquid Trichloromethane. *Mol. Phys.* **1990**, *71*, 1205–1221.

(24) Kanakubo, M.; Nanjo, H.; Nishida, T.; Takano, J. Density, viscosity, and electrical conductivity of N-methoxymethyl-N-methylpyrrolidinium bis(trifluoromethanesulfonyl)amide. *Fluid Phase Equilib.* **2011**, *302*, 10–13.

(25) In previous work, we have given a value of ± 0.000 05 $g \cdot cm^{-3}$ for the expanded uncertainty for the Anton-Paar DMA5000. However fits of simple polynomials in the temperature generally show larger residuals in the viscosity range 200−300 mPa·s, that is below 10 °C for $[Pyr_{14}][Tf_2N]$ and, we estimate between (10 and 30) °C for $[3\text{-}ABN_{13}][Tf_2N]$. This is the region where the two in-built viscosity corrections, one for nominal viscosities <700 mPa·s and one for those >500 mPa·s, coincide. So we have doubled the expanded uncertainty in this case. We have observed the same effect in data published by other workers who have used this instrument, e.g. ref 23.

(26) López, E. R.; Fernández, J. *Personal communication*, 30 Nov. 2010.

(27) Pereiro, A. B.; Veiga, H. I. M.; Esperança, J. M. S. S.; Rodríguez, A. Effect of Temperature on the Physical Properties of Two Ionic Liquids. *J. Chem. Thermodyn.* **2009**, *41*, 1419–1423.

(28) Kolbeck, C.; Lehmann, J.; Lovelock, K. R. J.; Kremer, T.; Paape, N.; Wasserscheid, P.; Fröba, A. P.; Maier, F.; Steinrück, A.-P. Density and Surface Tension of Ionic Liquids. *J. Phys. Chem. B* **2010**, *114*, 17025–17036.

(29) Shamsipur, M.; Beigi, A. A. M.; Teymouri, M.; Poumortazavi, S. M.; Irandoust, M. Physical and Electrochemical Properties of Ionic Liquids 1-Ethyl-3-imidazolium Tetrafluoroborate, 1-Butyl-3-methylimidazolium Trifluoromethanesulfonate and 1-Butyl-1-methylpyrrolidinium Bis(trifluoromethylsulfonyl)imide. *J. Mol. Liq.* **2010**, *157*, 43–50.

(30) Troncoso, J.; Cerdeiriña, C. A.; Navia, P.; Sanmamed, Y. A.; González-Salgado, D.; Romaní, L. Unusual Behavior of the Thermodynamic Response Functions of Ionic Liquids. *J. Phys. Chem. Lett.* **2010**, *1*, 211–214.

(31) Angell, C. A. Formation of Glasses from Liquids and Biopolymers. *Science* **1995**, *267*, 1924–1935.

(32) Salminen, J.; Papaiconomou, N.; Kumara, R. A.; Lee, J.-M.; Kerr, J.; Newman, J.; Prausnitz, J. M. Physicochemical Properties and Toxicities of Hydrophobic Piperidinium and Pyrrolidinium Ionic Liquids. *Fluid Phase Equilib.* **2007**, *261*, 421–426.

(33) Kunze, M.; Jeong, S.; Paillard, E.; Winter, M.; Passerini, S. Melting Behaviour of Pyrrolidinium-based Ionic Liquids and their Binary Mixtures. *J. Phys. Chem. C* **2010**, *114*, 12364–12369.

(34) Pan, Y.; Boyd, L. E.; Kruplak, J. F.; Cleland, W. E., Jr; Wilkes, J. S.; Hussey, C. L. Physical and Transport Properties of Bis(trifluoromethylsulfonyl)imide-based Room-Temperature Ionic Liquids: Application to the Diffusion of Tris(2,2́-bipyridyl)ruthenium(II). *J. Electrochem. Soc.* **2011**, *158*, F1–F9.

(35) Tokuda, H.; Ishii, K.; Susan, M. A. B. H.; Tsuzuki, S.; Hayamizu, K.; Watanabe, M. Physicochemical Properties and Structures of Room-Temperature Ionic Liquids. 3. Variation of Cationic Structures. *J. Phys. Chem. B* **2006**, *110*, 2833–2839.

(36) Castiglione, F.; Moreno, M.; Raos, G.; Famulari, A.; Mele, A.; Appetecchi, G. B.; Passerini, S. Structural Organization and Transport Properties of Novel Pyrrolidinium-Based Ionic Liquids with Perfluoroalkyl Sulfonylamide Anions. *J. Phys. Chem. B* **2009**, *113*, 10750–10759.

(37) Comminges, C.; Bahrdadi, R.; Laurent, M.; Troupel, M. Determination of Viscosity, Ionic Conductivity, and Diffusion Coefficients in Some Binary Systems: Ionic Liquids + Molecular Solvents. *J. Chem. Eng. Data* **2006**, *51*, 680–685.

(38) Wachter, P.; Schreiner, C.; Schweiger, H.-G.; Gores, H. J. Determination of Phase Transition Points of Ionic Liquids by Combination of Thermal Analysis and Conductivity Measurements at Very Low Heating and Cooling Rates. *J. Chem. Thermodyn.* **2010**, *42*, 900–903.

(39) Annat, G.; MacFarlane, D. R.; Forsyth, M. Transport Properties in Ionic Liquids and Ionic Liquid Mixtures: The Challenges of

Pulsed Field Gradient Measurements. *J. Phys. Chem. B* **2007**, *111*, 9018–9024.

(40) Martinelli, A.; Matic, A.; Jacobsson, P.; Börjesson, L.; Fernicola, A.; Scrosati, B. Phase Behaviour and Ionic Conductivity in Lithium Bis(trifluoromethylsulfonyl)imide-doped Ionic Liquids of the Pyrrolidinium Cation and Bis(trifluoromethylsulfonyl)imide Anion. *J. Phys. Chem. B* **2009**, *113*, 11247–11251.

(41) Johannson, P.; Fast, L. E.; Matic, A.; Appetechi, G. B.; Passerini, S. The Conductivity of the Pyrrolidinium and Sulfonylimide-based Ionic Liquids: A Combined Experimental and Computational Study. *J. Power Sources* **2010**, *195*, 2074–2076.

(42) Harris, K. R. Relations between the Fractional Stokes-Einstein and Nernst-Einstein equations and Velocity Correlation Coefficients in Ionic Liquids and Molten Salts. *J. Phys. Chem. B* **2010**, *114*, 9572–9577.

(43) Alba-Simionesco, C.; Cailliaux, A.; Alegría, A.; Tarjus, G. Scaling Out the Density Dependence of the α Relaxation in Glass-forming Polymers. *Europhys. Lett.* **2004**, *68*, 58–64.

(44) Casalini, R.; Mohanty, R.; Roland, C. M. Thermodynamic Interpretation of the Scaling of the Dynamics of Supercooled Liquids. *J. Chem. Phys.* **2006**, *125*, 014505−1–014505−9.

(45) Schrøder, T.; Bailey, N. P.; Pedersen, U. R.; Gnan, N.; Dyre, J. C. Pressure-energy Correlations in Liquids. III. Statistical Mechanics and Thermodynamics of Liquids with Hidden Scale Invariance. *J. Chem. Phys.* **2009**, *131*, 234503-1–234504-17.

(46) (a) Voronel, A.; Veliyulin, E.; Machavariani, V. Sh.; Kisliuk, A.; Quitmann, D. Fractional Stokes-Einstein Law for Ionic Transport in Liquids. *Phys. Rev. Lett.* **1998**, *80*, 2630–2633. (b) Veliyulin, E.; Shasha, E.; Voronel, A.; Machavariani, V. Sh.; Seifer, Sh.; Rosenberg, Yu.; Shumsky, M. G. Universal Transport Coefficient Behaviour in Ionic Melts. *J. Phys.: Condens. Matter* **1999**, *11*, 8773–8784.

(47) Harris, K. R. The Fractional Stokes−Einstein Equation: Application to Lennard-Jones, Molecular, and Ionic Liquids. *J. Chem. Phys.* **2009**, *131*, 054503−1–054503−8.

(48) Harris, K. R.; Kanakubo, M. Paper in preparation.

(49) Hayamizu, K.; Tsuzuki, S.; Seki, S.; Fujii, K.; Suenaga, M.; Umebayashi, Y. Studies on the Translational and Rotational Motions of Ionic Liquids Composed of N-methyl-N-propyl-pyrrolidinium (P-13) cation and Bis(trifluoromethanesulfonyl)amide and Bis(fluorosulfonyl)-amide Anions and Their Binary Systems Including Lithium Salts. *J. Chem. Phys.* **2010**, *133*, 194505/1–194505/13.

(50) Reference 51 reports similar behavior for $[Pyr_{13}][Tf_2N]$. Those of ref 49 conform to the expected Litovitz temperature dependence, whereas those of ref 51 do not. Further, the anion and cation plots cross, which is very unusual. Therefore it is possible that the diffusion results of ref 53 are in error.

(51) Wu, T.-Y.; Su, G.-S.; Wang, H. P.; Lin, Y.-C.; Gung, S.-T.; Lin, M.-W.; Sun, I.-W. Electrochemical Studies and Self Diffusion Coefficients in Cyclic Ammonium Based Ionic Liquids with Allyl Substituents. *Electrochim. Acta* **2011**, *56*, 3209–3218. Corrected data, Wu, T.-Y., *personal communication*, 9 May 2011.

(52) Seki, S.; Hayamizu, K.; Tsuzuki, S.; Fujii, K.; Umebayashi, Y.; Mitsugi, T.; Kobayashi, T.; Ohno, Y.; Kobayashi, Y.; Mita, Y.; Miyashiro, H.; Ishiguro, S. Relationships between Center Atom Species (N,P) and Ionic Conductivity, Density, Self-diffusion Coefficient of Quaternary Cation Room-temperature Ionic Liquids. *Phys. Chem. Chem. Phys.* **2009**, *11*, 3509–3514.

(53) Schönert, H. Evaluation of Velocity Correlation Coefficients from Experimental Transport Data in Electrolytic Systems. *J. Phys. Chem.* **1984**, *88*, 3359–3363.

(54) Tasseven, Ç.; Trullàs, J.; Alcaraz, O.; Silbert, M.; Giró, A. Static Structure and Ionic Transport in Molten AgBr and AgCl. *J. Chem. Phys.* **1997**, *106*, 7286–7294.

(55) Berne, B.; Rice, S. A. On the Kinetic Theory of Dense Fluids. XVI. The Ideal Ionic Melt. *J. Chem. Phys.* **1964**, *40*, 1347–1362.

(56) Supporting Information, ref 7, Tables S11 to S16.

(57) Ishida, T. Molecular Dynamics Study of the Dynamical Behaviour in Ionic Liquids through Interionic Interactions. *J. Non-Cryst. Solids* **2011**, *357*, 454–462.

(58) Friedman, H. L.; Mills, R. Velocity Cross Correlations in Binary Mixtures of Simple Fluids. *J. Solution Chem.* **1981**, *10*, 395–409.

(59) Ben-Amotz, D; Stell, G. Analytical Implementation and Critical Tests of Fluid Thermodynamic Perturbation Theory. *J. Chem. Phys.* **2003**, *119*, 10777–10788.

(60) Fragiadakis, D.; Roland, C. M. On the Density Scaling of Liquid Dynamics. *J. Chem. Phys.* **2011**, *134*, 044504−1–044504−3.

(61) Harris, K. R. Temperature and Pressure Dependence of the Viscosities of 2-EthylhexylBenzoate, Bis(2-ethylhexyl) Phthalate, 2,6,10,15,19,23-Hexamethyltetracosane (Squalane), and Diisodecyl Phthalate. *J. Chem. Eng. Data* **2009**, *54*, 2729–2738.

(62) Gnan, N.; Schrøder, T.; Pedersen, U. R.; Bailey, N. P.; Dyre, J. C. Pressure-energy Correlations in Liquids. IV. "Isomorphs" in Liquid Phase Diagrams. *J. Chem. Phys.* **2009**, *131*, 234504-1–234504-18.